Intelligent registration techniques of power equipment's using data fusion of contour-based infrared and visible data

Gang Yang and Na Zhang*

State Grid Shanxi Electric Power Research Institute,
Taiyuan, Shanxi, 030001, China
Email: yanggang9800@163.com
Email: xiedongnan@ldy.edu.rs
*Corresponding author

Shucai Li

State Grid Shanxi Lvliang Power Supply Company,
Lvliang, Shanxi, 033000, China
Email: louyimei@ldy.edu.rs

Fan Hu, Jichong Liang and Dawei Wang

State Grid Shanxi Electric Power Research Institute,
Taiyuan, Shanxi, 030001, China
Email: hitszhufan@163.com
Email: liangjichong@sx.sgcc.com.cn
Email: davidsgcc@126.com

Abstract: This paper proposes an automatic registration method for power equipment images using contour centreline main orientation features. Addressing low accuracy caused by scale/viewpoint variations in multi-modal images (infrared and visible), the method detects contour corner points as feature points, assigns scale/viewpoint-invariant orientation features through centreline analysis, and employs improved scale-invariant feature transform (SIFT) descriptors with connecting-line consistency matching to determine transformation parameters. Experimental results demonstrate registration errors of 2.742 and 2.543 in scenarios with subtle and significant viewpoint differences respectively, outperforming traditional SIFT, speeded-up robust features (SURF) and partial intensity invariant feature descriptor (PIIFD) methods. This approach effectively resolves complex-scenario registration challenges, providing an effective solution for intelligent monitoring of power equipment.

Keywords: infrared and visible image; image registration; contour centreline; feature matching.

Reference to this paper should be made as follows: Yang, G., Zhang, N., Li, S., Hu, F., Liang, J. and Wang, D. (2025) 'Intelligent registration techniques of power equipment's using data fusion of contour-based infrared and visible data', *Int. J. Information and Communication Technology*, Vol. 26, No. 20, pp.1–18.

Copyright © The Author(s) 2025. Published by Inderscience Publishers Ltd. This is an Open Access Article distributed under the CC BY-NC-ND license. (http://creativecommons.org/licenses/by-nc-nd/4.0/)

RETRACTED

Biographical notes: Gang Yang is a Senior Engineer. He worked in State Grid Shanxi Electric Power Research Institute. His research interests include intelligent diagnosis technology for power equipment status.

Na Zhang is a Senior Engineer. She worked in State Grid Shanxi Electric Power Research Institute. Her research interests include visual intelligent diagnosis technology for power equipment.

Shucai Li is an Engineer. He worked in State Grid Shanxi Lvliang Power Supply Company. His research interests include power equipment testing technology.

Fan Hu is a Senior Engineer. He worked in State Grid Shanxi Electric Power Research Institute. His research interests include intelligent recognition technology for power image.

Jichong Liang is a Senior Engineer. He worked in State Grid Shanxi Electric Power Research Institute. His research interests include state evaluation technology for substation equipment.

Dawei Wang is an Engineer. He worked in State Grid Shanxi Electric Power Research Institute. His research interests include electric power visual security prevention and control technology.

RETRACTED

1 Introduction

In order to meet the user ‘s increasing demand for electricity and the safe operation of the power system, the research and development of intelligent monitoring methods and self-diagnosis systems for power equipment has become a key link in the construction of ubiquitous power internet of things (Shi et al., 2020; Zaeri and Qasim, 2024; Jiang et al., 2019). With the development of various substation inspection robots and transmission line operation and maintenance UAV equipment based on infrared and visible light images, the power equipment self-diagnosis system shows great potential in terms of efficiency and autonomy, and is an effective method to reduce labour costs (Xu et al., 2018; Li et al., 2019b).

The existing infrared and visible image registration methods can be divided into three categories: calibration parameter-based, region-based and feature-based (Guo et al., 2021; Shen et al., 2020; Chen et al., 2020; Wen et al., 2022; Jin et al., 2016; Zhang et al., 2019; Zhao and Zhang, 2020). The method based on calibration parameters is a non-automatic registration method, which can only register a set of images taken at the same time, and its registration accuracy depends on the accuracy of calibration parameters. The region-based registration method relies on the linear correlation degree of image grey level and the overlap degree of visual field, and has poor adaptability and high computational complexity to complex scenes with differences in viewing angles, spectra and distortions. For example, the registration method based on gradient mutual information proposed in Xia and Yi (2018) and Li et al. (2019a). Si et al. (2024) proposed a registration algorithm for thermal infrared and visible apple images using an active contour model and feature point matching. The method achieves high accuracy with a

96% alignment success rate, outperforming existing approaches in precision and root mean square error.

The registration method based on point features has been widely used and studied, and it has strong robustness to complex image registration scenarios. The scale invariant feature transform (SIFT) method proposed in Lowe (2004) lays the foundation for the registration method framework based on point features. In Chen and Hao (2011), gradient inversion method and wheel contour feature point extraction method are introduced to realise heterogeneous image registration. Chen et al. (2010) proposed a calculation method based on square gradient principal direction and partial intensity invariant feature descriptor (PIIFD). In Dai et al. (2019), the preprocessing of PIIFD method is improved, and the similarity between infrared image and visible image is improved by combining the preprocessing method of image frequency domain decomposition. In Xu et al. (2017), Luo et al. (2020), Ji et al. (2014), Bay et al. (2006) and Mei and Yao (2019), faster infrared and visible image registration is achieved by improving the speeded up robust feature (SURF) method, and the computational complexity is lower than SIFT and PIIFD. Jiang et al. (2020) proposed an automatic registration method (CAO-C2F) for infrared and visible images of power equipment, using contour angle orientation (CAO) based on contour features to achieve viewpoint and scale invariance. Experiments show it outperforms existing methods in precision, recall, and root-mean-square error. However, the above existing image registration methods rely on the gradient of the image, and the registration accuracy is low in the scene where there are scale and angle differences between the infrared image and the visible image, resulting in a low correlation of the main direction descriptor, and ultimately unable to accurately match the infrared image and the visible image.

In view of the above problems, this paper proposes an automatic registration method of infrared and visible light images based on image contour features. The important contour features of infrared and visible light images of power equipment are taken as the core feature points, and the feature direction of the midline of the contour is taken as the main direction of the feature points. The improved SIFT operator is combined with the proposed consistency matching method to obtain the image matching points. By performing least squares fitting on the matching points, the mapping parameters between the infrared image and the visible light image are obtained, which solves the registration problem when there are scale and angle differences between the infrared and visible light images.

2 Contour centreline feature main direction assignment

Specifying the main direction for feature points is an important step to achieve scale and angle invariance. In order to realise the scale and angle invariance of infrared and visible images of power equipment, this paper proposes a marking method that uses the contour midline as the main direction of the feature.

2.1 Curvature scale space

The pixel coordinate set of the original contour curve in a single image is defined as

RETRACTED

$$l = \left\{ \Gamma^j \middle| \Gamma^j = \left\{ P_1^j, P_2^j, \ldots, P_n^j \right\} \right\} \frac{n_\Gamma}{j=1} \tag{1}$$

where Γ^j represents the j contour, $P_i^j = (x_i^j, y_i^j)$ represents the i pixel on the j contour, n is the number of pixels contained in the j contour, n_Γ is the number of contours contained in the image.

The contour curve in the image is generally expressed as a curve on the plane. The parameter equation of the plane curve $y = f(x)$ with curvature K is:

$$\begin{cases} y = \omega(t) \\ x = \psi(t) \end{cases} \tag{2}$$

$$K = \frac{\left| \psi'(t)\omega''(t) - \psi''(t)\omega'(t) \right|}{\left[\psi'^2(t) + \omega'^2(t) \right]^{\frac{3}{2}}} \tag{3}$$

Before using equation (3) to calculate the curvature of the contour curve Γ^j, considering the existence of burrs and noise in Γ^j, the Gaussian function of the scale parameter σ is used to smooth the Γ^j, that is:

$$\begin{cases} \Gamma_\sigma^j = \left\{ \left(X_\sigma^j, Y_\sigma^j \right) \right\} \\ X_\sigma^j = \left\{ x_i^j \right\}_{i=1}^n \otimes G_\sigma \\ Y_\sigma^j = \left\{ y_i^j \right\}_{i=1}^n \otimes G_\sigma \\ G_\sigma = \dfrac{e^{-\frac{x^2}{2\sigma^2}}\Big|_{x=-w}, -w+1, \ldots, 0, \ldots, w}{\sum_{x=-w}^{x=w} e^{-\frac{x^2}{2\sigma^2}}} \end{cases} \tag{4}$$

where G_σ is a one-dimensional Gaussian kernel function, and ⊗ represents the convolution operation.

Therefore, the curvature K of the contour curve Γ_σ^j is as follows:

$$K = \frac{\left| X_\sigma' Y_\sigma'' - X_\sigma'' \dot{Y} \right|}{\left(X_\sigma'^2 + Y_\sigma'^2 \right)^{\frac{3}{2}}} \tag{5}$$

2.2 Main direction of contour midline feature

The set of feature points detected in the curvature scale space in the image is denoted as $P_F = \{(x_i, y_i)\}_{i=1}^{nf}$ and the feature points located on the contour Γ^j are denoted as $P_f^j = (x_f^j, y_f^j j) \in P_F$. The eigenvectors of P_f^j pointing to the starting and ending neighbourhoods of Γ^j are defined as:

$$\begin{cases} \boldsymbol{\rho}_{f,b}^j = \left(x_{f,b}^j - x_f^j, y_{f,b}^i - y_f^j \right) \\ \left(x_{f,b}^j, y_{f,b}^j \right) = \boldsymbol{H}_b \cdot \left(X_\sigma^j(i), Y_\sigma^j(i) \right)\Big|_{i=f-\lambda_i+1,\ldots,f-1,f} \end{cases} \tag{6}$$

RETRACTED

$$\begin{cases} \boldsymbol{\rho}_{f,e}^{j} = \left(x_{f,e}^{j} - x_{f}^{j},\, y_{f,e}^{j} - y_{f}^{j}\right) \\ \left(x_{f,e}^{j},\, y_{f,e}^{j}\right) = \boldsymbol{H}_{e} \cdot \left(X_{\sigma}^{j}(i),\, Y_{\sigma}^{j}(i)\right)\Big|_{i=f,f+1,\cdots,f+\lambda_{e}-1} \end{cases} \tag{7}$$

where $f \in [1, n]$; $\rho_{f,b}^{j}$ and $\rho_{f,e}^{j}$ are the feature vectors of the feature points pointing to the beginning and end of the contour, respectively. λ_b and λ_e are the neighbourhood lengths of the feature points pointing to the beginning and end of the contour, respectively. H_b and H_e are the corresponding weighted row matrices.

Since the feature point is at the local maximum value of curvature, the feature vector at the beginning and end can be surrounded into a feature triangle. The direction vector pointed by the centreline corresponding to the feature point P_f^j is denoted as:

$$\rho_{f,m}^{j} = \left(x_{f,m}^{j},\, y_{f,m}^{j}\right) = \rho_{f,b}^{j} + \rho_{f,e}^{j} \tag{8}$$

The direction of the midline vector is assigned as the main direction of the feature point, which is the main direction of the contour midline feature proposed in this paper, and is expressed as follows:

$$\phi\left(P_{f}^{j}\right) = \begin{cases} \tan^{-1}\left(y_{f,m}^{j} \big/ x_{f,m}^{j}\right), & y_{f,m}^{j} \geqslant \cap\, x_{f,m}^{j} \geqslant 0 \\ \tan^{-1}\left(y_{f,m}^{j} \big/ x_{f,m}^{j}\right), & x_{f,m}^{j} < 0 \\ \tan^{-1}\left(y_{f,m}^{j} \big/ x_{f,m}^{j}\right), & y_{f,m}^{j} < 0 \cap x_{f,m}^{j} > 0 \end{cases} \tag{9}$$

where $\phi(P_f^j)$ has the range $[0, 2\pi)$.

Finally, in order to make the main direction calculation method realises the scale invariance of the image, the key parameters λ_b and λ_e are assigned adaptively in this paper. λ_b takes the number of pixels between the feature point P_f^j and the nearest curvature local minimum point pointing to the beginning of the contour. Similarly λ_e takes the number of pixels between the feature point P_f^j and the nearest local minimum of curvature pointing to the end of the contour. The respective weighted row matrices H_b and H_e are set as average weighted, that is:

$$H_{b,e} = \frac{[1 \quad 1 \quad \cdots \quad 1]}{\lambda_{b,e}} \tag{10}$$

The significance of the main direction assignment of the contour feature vector is that the feature point is the vertex, the feature vector pointing to the beginning and end of the contour is the edge, and the direction of the centreline of the triangle is the main direction of the feature point P_f^j, as shown in Figure 1.

The adaptive values of λ_b and λ_e make the sampling contour of the same feature point at different scales similar, that is, the feature triangles are similar, which ensures that the midline feature vectors refer to the same direction.

The higher the accuracy of the main direction assignment of the same feature points in the image to be registered, the higher the correlation of the feature descriptors between

RETRACTED

the same feature points, and the more correct matching points are further screened out. The main direction calculation method proposed in this paper does not rely on the similarity between the grey levels of infrared and visible light images, but focuses on the contour line features of images with higher similarity. Therefore, it can solve the problem that the similarity of image gradient statistical histogram is too low due to the large difference of image spectrum and resolution caused by SIFT, SURF and other methods.

Figure 1 Main direction of contour midline feature (see online version for colours)

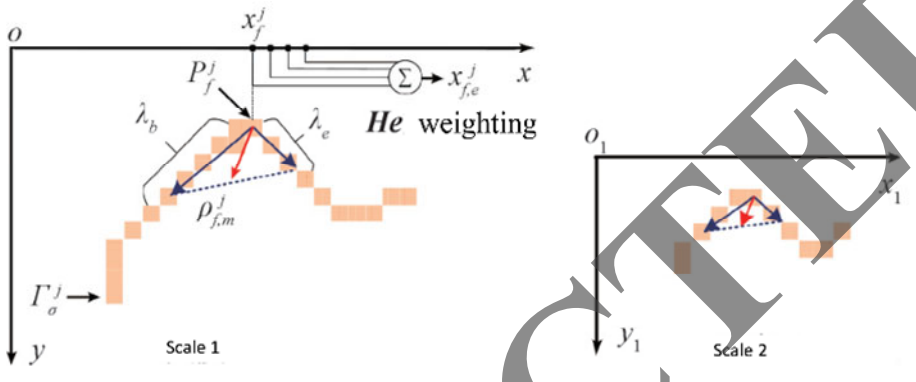

3 Connection consistency feature matching

Feature matching aims to screen out the corresponding feature points in the infrared and visible images of power equipment to calculate the transformation parameters between images. In this paper, a line consistency feature matching method is proposed to achieve accurate matching between feature points of infrared and visible images.

3.1 Connection consistency

The infrared image is horizontally concatenated with the visible light image after rotation and scale transformation. In theory, when the infrared and visible light images have the same scale and no relative rotation, the tilt angle and length of the connecting lines between all correctly matched feature points in the concatenated image are equal, while the tilt angle and length of the connecting lines between incorrectly matched points are different from those of correctly matched points. This property is defined as connection consistency in this article, as shown in Figure 2. The white solid line connects the correct matching points, while the white dashed line connects the incorrect matching points.

Assuming ξ is the scale of visible light relative to infrared images (i.e., the scaling factor of the pixel area of the same target in the images), the set of candidate matching feature points corresponding to this scale is denoted as

$$\begin{cases} P_1 = \left\{ p_{1i} \middle| p_{1i} = (x_{1i}, y_{1i}) \right\}_{i=1}^{n_p} \\ P_2 = \left\{ p_{2i} \middle| p_{2i} = (x_{2i}, y_{2i}) \right\}_{i=1}^{n_p} \end{cases} \tag{11}$$

RETRACTED

where P_1 and P_2 are matching points of infrared and visible images respectively; n_p is the number of matching points.

Figure 2 Schematic diagram of connecting line consistency of feature points (see online version for colours)

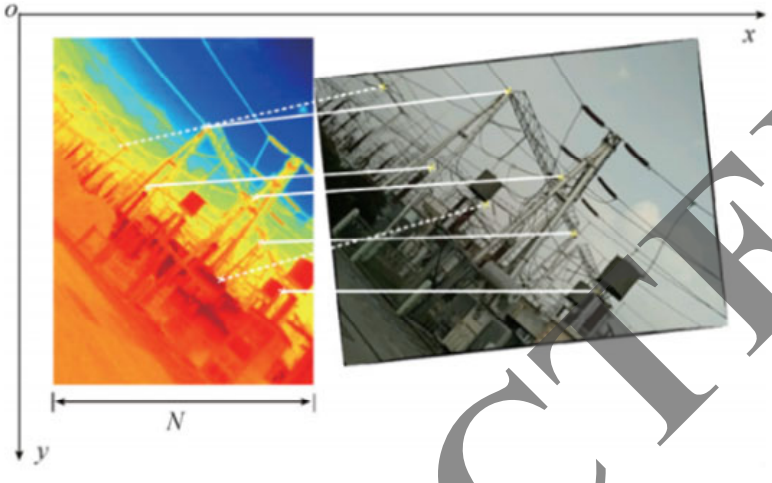

Further, assuming that the rotation angle of the visible light image relative to the infrared image is $-\phi_R$, P_2 is rotated ϕ_R and scaled to the infrared image scale, and the transformed visible light candidate matching point P_{2R} is as follows:

$$P_{2R} = \left\{ p'_{2i} \middle| p'_{2i} = \left(x'_{2i}, y'_{2i} \right) = \xi p_{2i} \mathbf{R} \right\}_{i=1}^{n_p} \tag{12}$$

$$\mathbf{R} = \begin{bmatrix} \cos\phi_R & -\sin\phi_R \\ \sin\phi_R & \cos\phi_R \end{bmatrix} \tag{13}$$

where $\mathbf{R}$ is the rotation transformation matrix.

The tilt angle set φ and the length set D of the corresponding matching feature point connection are respectively:

$$\begin{cases} \varphi = \left\{ \varphi_i \middle| \varphi_i = \tan^{-1}\left(\dfrac{y'_{2i} - y_{1i}}{x'_{2i} + N - x'_{1i}} \right) \right\}_{i=1}^{n_p} \\ D = \left\{ d_i \middle| d_i = \left\| x'_{2i} + N - x'_{1i},\ y'_{2i} - y'_{1i} \right\| 2 \right\}_{i=1}^{n_p} \end{cases} \tag{14}$$

where N is the horizontal resolution of the infrared image.

In the first-stage coarse alignment, the best matching φ and D are selected based on the visible light contour map and the infrared contour map, and the corresponding feature points p_{1i} and p_{1j} from the visible light and infrared contour maps are matched. The feature points $\varphi_i = \varphi_j$, $d_i = d_j$.

RETRACTED

3.2 Line consistency matching method

The process of the connection consistency matching method proposed in this paper is shown in Figure 3, and the specific steps are as follows:

1 Obtaining initial matching points by bilateral matching: after generating a set of descriptors of infrared image feature points and multiple sets of descriptors of visible image feature points at multiple scales, a set of infrared and multiple sets of visible image feature descriptors are matched by bilateral matching method to obtain candidate matching feature points of single-scale infrared and visible images at all scales.

2 Voting strategy to obtain the best scale: according to the characteristics of feature descriptors, the descriptors of the same feature point in the same scale infrared and visible light images are the most similar. Therefore, the scale with the largest number of candidate matching points in the result of step 1 is regarded as the best matching scale of infrared and visible light images. The scale value is the scale ξ in equation (12), and the best candidate matching point pairs corresponding to this scale are P_1 and P_2 in equation (11). There are a large number of mismatching points in the candidate matching points that need to be removed.

3 Remove significant error points: note that the principal direction sets of the two groups of feature points corresponding to P_1 and P_2 are $\phi_1 = \{\phi(p_{1i})\}_{i=1}^{n_p}$ and $\phi_2 = \{\phi(p_{2i})\}_{i=1}^{n_p}$ and the visible light relative to infrared is obtained by subtracting ϕ_1 and ϕ_2:

$$\Delta\phi = \left\{\Delta\phi_i \middle| \Delta\phi_i = \phi(p_{2i}) - \phi(p_{1i})\right\}_{i=1}^{n_p} \tag{15}$$

The interval [0, 360°) is divided into 72 intervals with a length of 5°, and the number of elements falling in each interval within $\Delta\phi$ is counted by histogram. The angle corresponding to the interval with the largest number of candidate rotation angles (if the maximum value corresponds to multiple adjacent intervals, the average value of each interval is taken) is regarded as the rotation angle of the visible image relative to the infrared image in equation (12). The inclination angle and length set φ and D corresponding to the feature point connection can be obtained from equation (13).

There may be some perspective differences between the images in the actual registration scene, which leads to the connection between the correct matching points is not strictly parallel and the length is equal. Considering the existence of this difference, the actual value φ_R of the inclination angle of the line between the correct matching points is obtained by using the same histogram statistical method as the calculation ϕ_R, the ratio of inclination angle error to length error is set to be ε_φ and ε_D. The point corresponding to the value in φ at the outer angle of the interval $[\varphi_R - \varepsilon_\varphi, \varphi_R + \varepsilon_\varepsilon]$ is regarded as the wrong matching point.

Then calculate the average length D_{mean} of the remaining matching points, and the point corresponding to the line whose value is outside the interval $[D_{mean}(1 - \varepsilon_D), D_{mean}(1 + \varepsilon_D)]$ in D is regarded as the wrong matching point. It should be noted that if the perspective difference between images is larger, it is necessary to set a larger tilt

RETRACTED

angle error ε_φ and length error ratio ε_D to retain more correct matching points as much as possible, but fewer false matching points are removed.

4 Random sample consensus (RANSAC) refinement: based on the coarse alignment contour map from step 3, the optimal coarse alignment contour map is selected. However, due to some isolated points or unreasonable matches in the contour map, a portion of the contour map contains significant noise. To address this, an outlier removal process is applied using the RANSAC method, which effectively filters out noise and obtains a refined contour map with fewer mismatches. By iteratively applying the RANSAC method, the contour map can be optimised to reduce noise significantly, ensuring the refined contour map does not introduce additional errors.

Figure 3 Flowchart of the connecting line consistency matching process (see online version for colours)

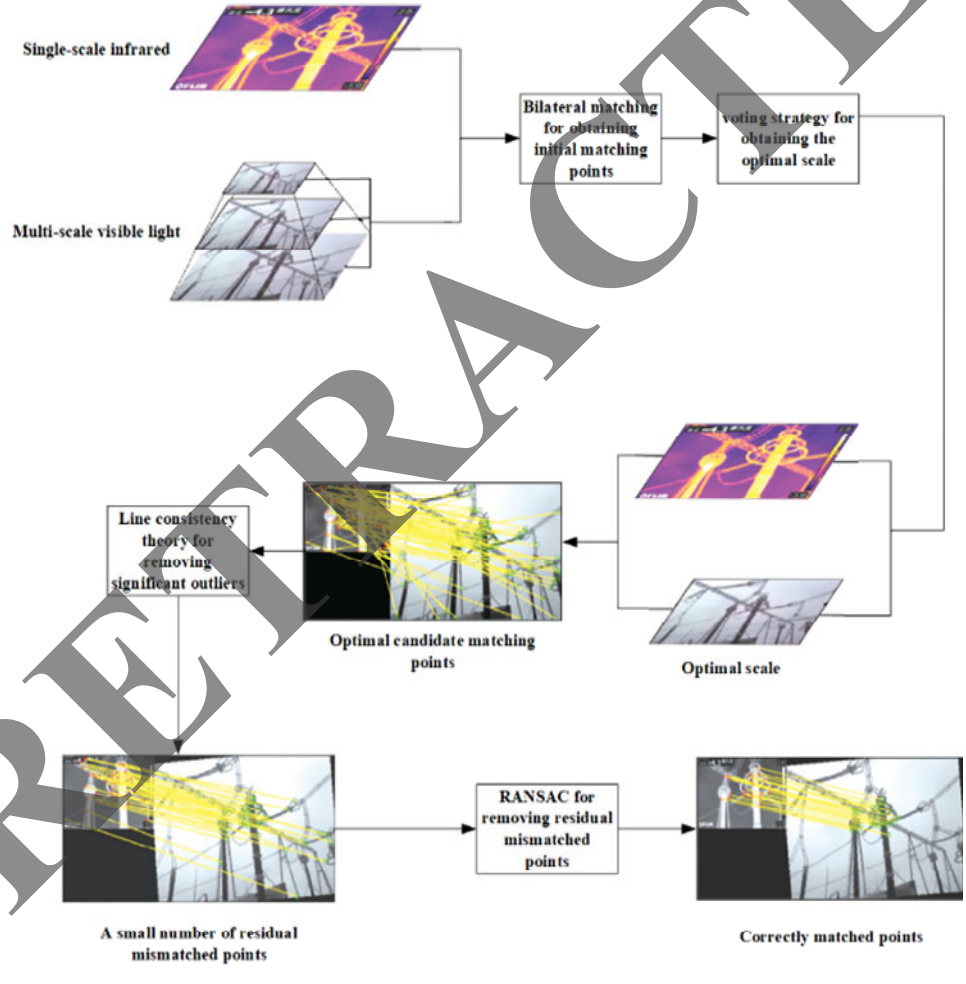

RETRACTED

Figure 4 Statistic histogram diagram of the number of candidate rotation angles in different angle intervals (see online version for colours)

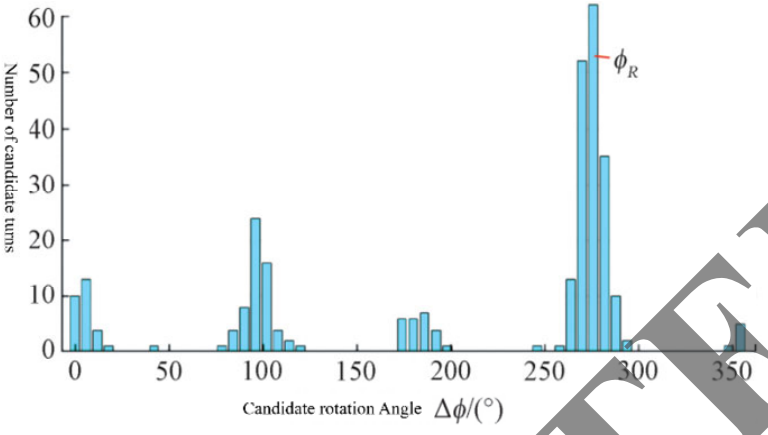

4 Registration process

The automatic registration algorithm proposed in this paper is shown in Figure 6, and is described as follows:

1 Image preprocessing: the input infrared and visible light source images are greyed, and the grey value range is linearly stretched to [0, 255] to enhance details of the image, and the image resolution is adjusted to the same longitudinal resolution;

2 Feature point extraction: the CSS corner point detection algorithm (Du et al., 2018) based on global and local curvature is used to extract corner points in infrared and visible images as the feature points of the image, and the contours midline feature main direction calculation method proposed in this paper is used to assign a unique main direction to each feature point.

Figure 5 CSS corner point detection algorithm flow

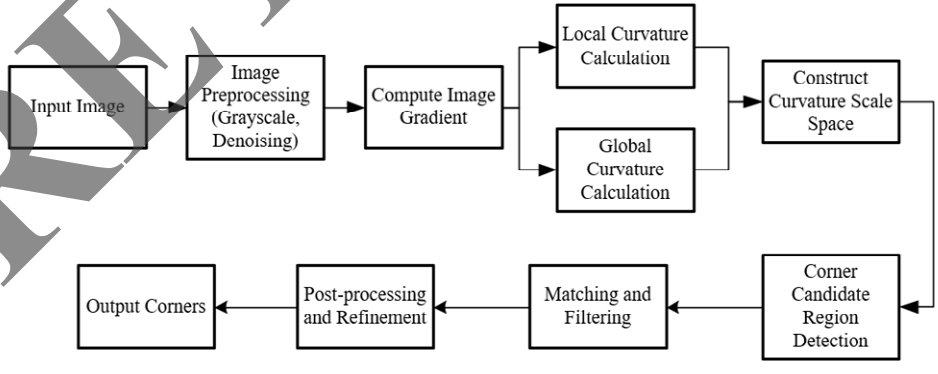

RETRACTED

3 Descriptor extraction: extract SIFT descriptors in the main direction of visible images under infrared and different scale sampling [the normalisation method in Chen et al. (2010) is used for segmented processing of SIFT] as the feature description of feature points.

4 Connection consistency feature matching: use the connection consistency matching method proposed in this paper to match feature descriptors and filter out the correct matching feature points.

5 Calculation of image space transformation parameters: the least square method is used to fit all the correct matching points to obtain the optimal projection transformation parameters between infrared and visible images.

Figure 6 The scheme of the proposed registration method (see online version for colours)

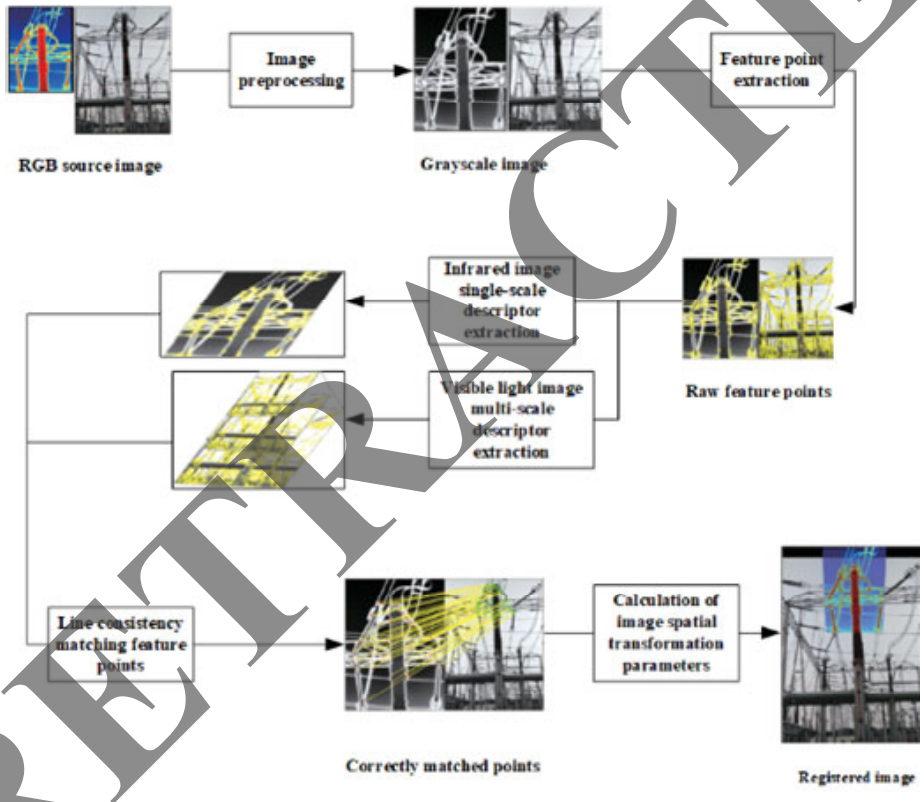

RETRACTED

5 Registration experiment results and analysis

5.1 Experimental platform and parameter setting

The experiments in this paper are based on Intel(R) Core(TM) i7-8550U CPU@1.90 GHz hardware platform and MATLAB R2020b platform. The algorithm in this paper is MATLAB programming code. The experimental source images were obtained from the

infrared and visible light image database of substation power equipment captured by inspection equipment, in which the infrared image resolution was 768 × 576, and the visible image resolution was 1,920 × 1,080. The resolution of the visible image is adjusted to 768 × 576 according to the original scale of the image.

The parameters of the algorithm in this paper are set as follows: $\varepsilon_\varphi = 20°$; $\varepsilon_D = 0.5$. The visible light multi-sampling scales are 0.5, 1.0 and 2.0.

5.2 Experimental evaluation index

Root mean square error (RMSE) is an important index to measure the positioning accuracy of matching points and the accuracy of the entire registration algorithm, which is defined as:

$$RMSE = \sqrt{\frac{1}{N_c}\sum_{i=1}^{N_c}\left\|(x_{1i}, y_{1i}) - (x_{2i}^c, y_{2i}^c)\right\|_2^2} \tag{16}$$

where (x_{1i}, y_{1i}) is the coordinates of matching points in infrared images; (x_{2i}^c, y_{2i}^c) is the theoretical matching point coordinates after the projection of the corresponding matching points in visible images by the manually calibrated reference transformation matrix; N_c is the number of matching point pairs.

In order to distinguish the positioning accuracy of each pair of matching points, the points satisfying $\left\|(x_{1i}, y_{1i}) - (x_{2i}^c, y_{2i}^c)\right\|_2 \leqslant 4$ are regarded as accurate matching points, and the points satisfying $4 < \left\|(x_{1i}, y_{1i}) - (x_{2i}^c, y_{2i}^c)\right\|_2 \leqslant 8$ are regarded as an inaccuracy point, and these are recorded as correct matching points. The points satisfying $\left\|(x_{1i}, y_{1i}) - (x_{2i}^c, y_{2i}^c)\right\|_2 > 8$ are considered false match points.

In order to measure the classification capability of descriptor matching algorithm, two important indicators, precision and recall, are introduced, which are defined as:

$$\begin{cases} \#\text{Correct} = \#\text{Accuracy} + \#\text{Inaccuracy} \\ \text{Precision} = \dfrac{\#\text{Correct}}{\#\text{Correct} + \#\text{False}} \\ \text{Recall} = \dfrac{\#\text{Correct}}{\#\text{Correspondences}} \end{cases} \tag{17}$$

where correspondences represents the number of original correct matching points in all corners extracted by CSS algorithm, the larger the values of precision and recall, the stronger the ability of the representative matching algorithm to distinguish the right and wrong matching points.

5.3 Registration results

In order to verify the effectiveness of the algorithm in this paper, the algorithms proposed in Gao et al. (2013), Dai et al. (2019), Xu et al. (2017, 2019) and Du et al. (2018) are compared with the algorithm in this paper. The four comparison algorithms and the algorithm in this paper belong to the matching algorithm based on point feature framework.

RETRACTED

5.3.1 Image registration comparison results without obvious angle difference

The registration results of different algorithms in five groups of image scenes without rotation and visual field difference are given in Table 1. It can be seen from the results that the algorithm in this paper successfully matches five groups of images with an average error of 2.742 pixels, and the matching accuracy and registration error are both optimal, and the recall rate is optimal or sub-optimal, while there are matching failures in Du et al. (2018).

Table 1 Comparison of registering the images with inapparent viewpoint differences by different methods

		Picture class				
Evaluation index		*Contrast algorithm*				
Precision	Docu (Gao et al., 2013)	1	2	3	4	5
	Docu (Dai et al., 2019)	0.933	0.033	0.923	0.926	0.875
	Docu (Xu et al., 2017)	0.796	0.714	0.875	0.735	0.778
	Docu (Du et al., 2018)	-	0.848	0.718	0.925	0.714
	Textual algorithm	*.936*	*1.000*	*0.946*	*1.000*	*0.988*
Recall	Docu (Gao et al., 2013)	*0.160*	0.067	0.117	0.065	*0.207*
	Docu (Dai et al., 2019)	0.061	0.044	0.069	0.037	0.071
	Docu (Xu et al., 2017)	0.036	0.003	0.025	0.017	0.021
	Docu (Du et al., 2018)	-	0.046	0.054	0.105	0.079
	Textual algorithm	0.117	*0.170*	*0.165*	*0.287*	0.098
RMSE	Docu (Gao et al., 2013)	10.843	92.085	9.798	9.839	11.576
	Docu (Dai et al., 2019)	15.111	16.243	11.891	16.618	14.225
	Docu (Xu et al., 2017)	7.994	9.674	8.510	8.627	7.867
	Docu (Du et al., 2018)	-	11.821	10.262	10.994	12.440
	Textual algorithm	*3.495*	*1.698*	*1.749*	*2.955*	*3.911*

By comparing the results of Gao et al. (2019) and the method presented in this paper, it can be seen that the main direction of contour midline feature used in this paper has higher registration accuracy than SIFT main direction used in Gao et al. (2019) when similar extraction methods of contour feature points and gradient feature descriptors are used. By comparing the results of the image grey space feature point extraction method used in Dai et al. (2019) and Du et al. (2018) with the PIIFD calculation method, it can be seen that the matching point positioning results obtained by the proposed algorithm are more accurate, which further verifies the superiority of the main direction allocation method proposed in this paper. Compared with the results of Guo et al. (2020), which used contour image as the image to be registered and SURF principal direction and descriptor, it can be seen that the method proposed in this paper based on contour features to extract feature points and assign principal direction has smaller registration errors.

From the comparison results of the number of correct matching points shown in Figure 7, it can be seen that the number of accurate matching points obtained by the proposed algorithm is much higher than that of other comparison algorithms, which verifies that the proposed algorithm has strong feature point matching performance.

RETRACTED

Figure 7 Comparison of the numbers of accurate matching points of registering the source images with inapparent viewpoint differences by different methods (see online version for colours)

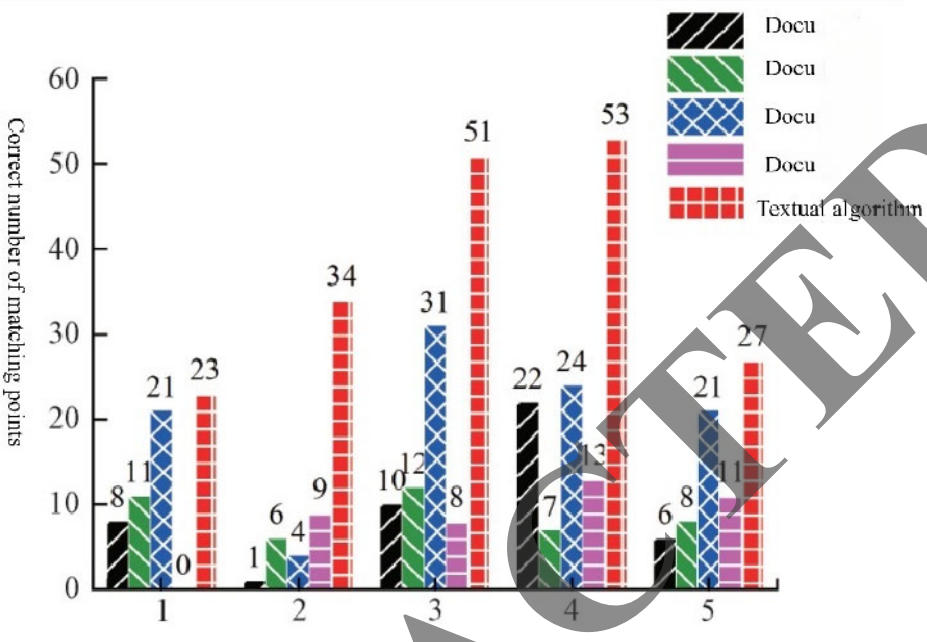

As can be seen from the image registration results of the proposed algorithm given in Figure 8, the colour mosaic images obtained by the proposed algorithm have high overlap and high smoothness at the image stitching, which verifies that the proposed algorithm can achieve high-precision registration. In Figure 8, the first behaviour is the result of source image matching points, and the second behaviour is the result of colour map mosaic.

Figure 8 Results of registering the images with inapparent viewpoint differences by the proposed method (see online version for colours)

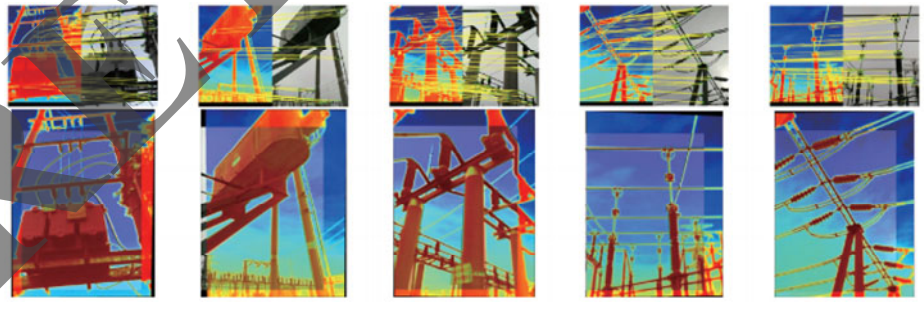

RETRACTED

5.3.2 Image registration comparison results with significant viewing angle differences

In the other five groups of matching experiments with significant visual field differences, the four algorithms failed to match successfully, so only the matching results of the algorithm presented in this paper are shown in Table 2 and Figure 9. The first behaviour is the result of source image matching points, and the second behaviour is the result of colour map mosaic. It can be seen from the results that the average matching error of this algorithm is 2.543. There is a large field of view rotation between the images or under perspective differences, the algorithm in this paper successfully matched five groups of images in complex scenes by relying on accurate principal direction calculation method, and showed the same high-precision registration results as in simple scenes. The overlap degree of fused images after matching was still high, and the connection of equipment components was smooth.

While the proposed contour centreline feature-based registration method excels in scenarios with viewpoint and scale differences, its robustness may slightly decrease in specific high-noise environments, such as images with fine speckles or very low contrast regions. This is because the method relies on contour feature extraction, where noise could interfere with corner detection accuracy. However, this limitation is minor in typical power equipment image scenarios and does not significantly impact overall performance.

Table 2 Result of registering the source images with apparent viewpoint differences by the proposed method

Evaluation index	*Picture class*				
	6	*7*	*8*	*9*	*10*
Precision	0.897	0.972	0.890	1.000	0.896
Recall	0.029	0.045	0.066	0.152	0.035
RMSE	2.906	2.928	1.476	1.818	3.537

Figure 9 Results of registering the images with apparent viewpoint differences by the proposed method (see online version for colours)

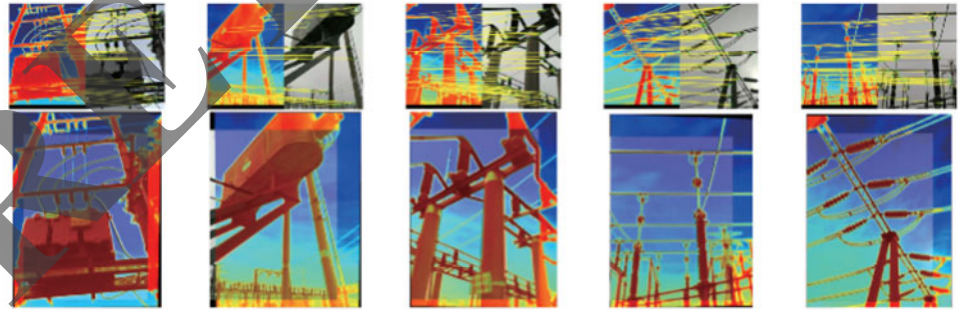

RETRACTED

6 Conclusions

In this study, we proposed an automatic registration method for infrared and visible images of power equipment based on contour centreline feature orientations, achieving significant advancements in registration accuracy and robustness. Experimental results demonstrate that the method attains average root mean square errors (RMSE) of 2.742 and 2.543 pixels in scenes with inapparent and apparent viewpoint differences, respectively, outperforming traditional methods such as SIFT, SURF and PIIFD, as well as other point feature-based approaches (e.g., Gao et al., 2013; Dai et al., 2019). The proposed contour midline feature assignment method ensures high perspective invariance, enabling successful registration even in complex scenarios where comparative algorithms fail. Additionally, the connection consistency matching technique effectively filters correct matching points, yielding high precision and recall rates, as evidenced by the increased number of accurate matches (Figure 7) and smooth, highly overlapping fused images (Figures 8 and 9). This approach provides a reliable and precise solution for infrared and visible image registration, enhancing the capabilities of automatic diagnostic systems for power equipment. Despite these achievements, the method's performance under extreme illumination conditions or highly cluttered backgrounds remains untested due to the limited diversity of experimental scenarios. Furthermore, its computational complexity may hinder real-time implementation on resource-constrained platforms. Future enhancements could focus on integrating deep learning techniques to improve robustness against environmental variations and optimising the algorithm's efficiency to meet the demands of real-time applications in power system monitoring.

Declarations

This work was supported by State Grid Shanxi Electric Power Company Technology Project: Research and application of precise diagnosis technology for infrared three-dimensional imaging and thermal anomalies (No. 52053023000Y).

The author declares that it does not have any known interests or personal relationships that could potentially influence the reported work in this paper.

References

Bay, H., Tuytelaars, T. and Van Gool, L. (2006) 'SURF: speeded up robust features', *Computer Vision–ECCV 2006: 9th European Conference on Computer Vision, Proceedings, Part I*, 7–13 May, Graz, Austria, Springer, Berlin Heidelberg, Vol. 3951, pp.404–417.

Chen, J., Tian, J., Lee, N., Zheng, J., Smith, R.T. and Laine, A.F. (2010) 'A partial intensity invariant feature descriptor for multimodal retinal image registration', *IEEE Transactions on Biomedical Engineering*, Vol. 57, No. 7, pp.1707–1718.

Chen, J.Q. and Hao, Y. (2011) 'An improved SIFT features reversed matching algorithm', *Microcomputer Information*, Vol. 27, No. 3, pp.209–211.

Chen, L., He, Y. and Dong, S. (2020) 'Recognition of hydraulic pump leakage status based on deep neural network', *Chinese Journal of Scientific Instrument*, Vol. 41, No. 4, pp.86–93.

Dai, J.D., Liu, Y.D., Mao, X.Y., Sheng, G.H. and Jiang, X.C. (2019) 'Registration based on NSCT-domain FAST corner detection for infrared and visible images of electrical equipment', *Electrical Measurement and Instrumentation*, Vol. 56, No. 1, pp.108–114.

RETRACTED

Du, Q., Fan, A., Ma, Y., Fan, F., Huang, J. and Mei, X. (2018) 'Infrared and visible image registration based on scale-invariant PIIFD feature and locality preserving matching', *IEEE Access*, Vol. 6, pp.64107–64121, https://doi.org/10.1109/ACCESS.2018.2877642.

Gao, J., Wu, Y., Wu, K. and Sun, J. (2013) 'Image matching method based on corner detection', *Chinese Journal of Scientific Instrument*, Vol. 34, No. 8, pp.1717–1725.

Guo, X., Xu, J. and Lu, W. (2021) 'The colour block registration method of fuzzy image under multi-layer P-spline geometric transformation', *International Journal of Information and Communication Technology*, Vol. 19, No. 1, pp.93–108.

Guo, X., Xu, J. and Lu, W. (2021) 'The colour block registration method of fuzzy image under multi-layer P-spline geometric transformation', *International Journal of Information and Communication Technology*, Vol. 19, No. 1, pp.93–108.

Ji, L.E., Yang, F.B. and Wang, Z.S. (2014) 'Bi-directional matching algorithm based on SURF features for visible and negative image of infrared image', *Opto-Electronic Engineering*, Vol. 41, No. 5, pp.77–82.

Jiang, Q., Liu, Y., Yan, Y., Deng, J., Fang, J., Li, Z. and Jiang, X. (2020) 'A contour angle orientation for power equipment infrared and visible image registration', *IEEE Transactions on Power Delivery*, Vol. 36, No. 4, pp.2559–2569.

Jiang, X., Liu, Y.D., Fu, X.F., Xu, P., Wang, S.J. and Sheng, G. (2019) 'Construction ideas and development trends of transmission and distribution equipment of the ubiquitous power internet of things', *High Voltage Engineering*, Vol. 45, No. 5, pp.1345–1351.

Jin, L.J., Tian, Z.H.R., Gao, K., et al. (2016) 'Discrimination of insulator contamination grades using information fusion of infrared and visible images', *Proceedings of the CSEE*, Vol. 36, No. 13, pp.3682–3691.

Li, L.J., Liu, X.H. and Huang, X.X. (2019a) 'Multispectral image registration based on symmetrical edge', *Semiconductor Optoelectronics*, Vol. 40, No. 3, pp.395–400.

Li, W., Wang, J. and Yu, Y. (2019b) 'An infrared automatic fault recognition method for electrical parts based on visible matching matrix', *Infrared Technology*, Vol. 41, No. 11, pp.1047–1056.

Lowe, D.G. (2004) 'Distinctive image features from scale-invariant keypoints', *International Journal of Computer Vision*, Vol. 60, No. 2, pp.91–110.

Luo, J.F., Qiu, G., Zhang, Y., Feng, S. and Han, L. (2020) 'Research on speeded up robust feature binocular vision matching algorithm based on adaptive double threshold', *Chinese Journal of Scientific Instrument*, Vol. 41, No. 3, pp.240–247.

Mei, M. and Yao, M. (2019) 'Feature extraction algorithm for fast moving pedestrians with frame drop constraint based on deep learning', *International Journal of Information and Communication Technology*, Vol. 15, No. 4, pp.331–343.

Shen, X.J., Yu, X.L., Wang, Y.D., et al. (2020) 'Research on three-dimensional visualization scheme of infrared thermal temperature measurement data for substation power equipment', *High Voltage Engineering*, Vol. 46, No. 8, pp.1–9.

Shi, J., Li, Z., Gu, C., Sheng, G. and Jiang, X. (2020) 'Research on foreign matter monitoring of power grid with faster R-CNN based on sample expansion', *Power System Technology*, Vol. 44, No. 1, pp.44–51.

Si, H., Wang, Y., Liu, Q., Li, W., Wan, L., Song, J., … and Sun, C. (2024) 'A registration algorithm for the infrared and visible images of apple based on active contour model', *The Visual Computer*, Vol. 40, No. 4, pp.2833–2855.

Wen, J.T., Wang, T., Sun, J.D., et al. (2022) 'Perimeter intrusion event identification of oil and gas pipelines under complex conditions based on deep transfer learning', *Chinese Journal of Scientific Instrument*, Vol. 43, No. 8, pp.12–19.

Xia, P. and Yi, H. (2018) 'Calibration of lidar and camera based on maximum mutual information', *Chinese Journal of Scientific Instrument*, Vol. 39, No. 1, pp.34–41.

RETRACTED

Xu, J.X., Lu, Q.W., Ma, Y.P. and Qian, R. (2017) 'Registration method between infrared and visible images of electrical equipment based on slope consistency', *Journal of Optoelectronics Laser*, Vol. 28, No. 7, pp.794–802.

Xu, P., Li, Z., Hong, T. and Ni, H. (2018) 'Fruit fly image segmentation and species determination algorithm', *International Journal of Information and Communication Technology*, Vol. 13, No. 2, pp.176–185.

Xu, P., Li, Z., Hong, T. and Ni, H. (2018) 'Fruit fly image segmentation and species determination algorithm', *International Journal of Information and Communication Technology*, Vol. 13, No. 2, pp.176–218.

Zaeri, N. and Qasim, R.R. (2024) 'Resilient recognition system for degraded thermal images using convolutional neural networks', *International Journal of Information and Communication Technology*, Vol. 25, No. 1, pp.50–71.

Zhang, Q., Wang, J. and Li, W. (2019) 'Insulator state detection of convolutional neural networks based on feedback mechanism', *Transactions of China Electrotechnical Society*, Vol. 34, No. 16, pp.3311–3321.

Zhao, H.S. and Zhang, Z.Y. (2020) 'Power equipment infrared and visible images registration based on cultural wolf pack algorithm', *Acta Optica Sinica*, Vol. 40, No. 16, p.1610003.

RETRACTED